NASA TECHNICAL NOTE

NASA TN D-4564

NASA TN D-4564

EXPERIMENTAL VERIFICATION OF A DOUBLE DEAD-TIME MODEL DESCRIBING CHUGGING IN LIQUID BIPROPELLANT ROCKET ENGINES

by John R. Szuch and Leon M. Wenzel

Lewis Research Center
Cleveland, Ohio

NATIONAL AERONAUTICS AND SPACE ADMINISTRATION • WASHINGTON, D. C. • MAY 1968

NASA TN D-4564

EXPERIMENTAL VERIFICATION OF A DOUBLE DEAD-TIME MODEL DESCRIBING CHUGGING IN LIQUID BIPROPELLANT ROCKET ENGINES

By John R. Szuch and Leon M. Wenzel

Lewis Research Center
Cleveland, Ohio

NATIONAL AERONAUTICS AND SPACE ADMINISTRATION

For sale by the Clearinghouse for Federal Scientific and Technical Information
Springfield, Virginia 22151 – CFSTI price $3.00

ABSTRACT

Stability limits were determined, experimentally, for a 2-inch (5.08 cm) diameter rocket engine. Liquid oxygen and gaseous hydrogen were the propellants. Chamber pressures of 650 and 300 psia (4.48×10^6 and 2.07×10^6 N/m^2) were run with an oxidant-fuel ratio of 5.0 and a characteristic length of 95 inches (2.41). For comparison with experimental data, boundaries were generated on the analog computer using the chugging model proposed by the authors and calculated values of delay. Results agreed with regard to observed frequencies and boundary shape. Discrepancies in boundary location (required pressure drops) were attributed to a high combustion noise level.

EXPERIMENTAL VERIFICATION OF A DOUBLE DEAD-TIME MODEL DESCRIBING CHUGGING IN LIQUID BIPROPELLANT ROCKET ENGINES

by John R. Szuch and Leon M. Wenzel

Lewis Research Center

SUMMARY

Low frequency combustion instabilities in liquid propellant rocket engines, commonly referred to as chugging, have been the subject of many analyses during the past two decades. The purpose of this investigation was to verify, experimentally, the chugging model previously proposed by the authors. The proposed double dead-time model considers each propellant to be acted upon by a discrete time delay between injection and burning in the combustion chamber. This differs from the commonly used single delay model where both propellants are acted upon by a single delay.

Use of the double dead-time model results in a stability boundary having several distinctive characteristics. More than one range of chugging frequencies may be observed along the boundary. Also, a reversal in slope of the boundary occurs at high fuel injector pressure drops, indicating the possibility of stabilization by decreasing the fuel injector pressure drop.

Stability boundaries were determined, experimentally, for a 2-inch (5.08 cm) diameter rocket engine. Liquid oxygen and gaseous hydrogen were the propellants. Boundaries were determined for two configurations: a chamber pressure of 650 psia (4.48×10^6 N/m^2), contraction ratio of 16.8, and a chamber pressure of 300 psia (2.07×10^6 N/m^2), contraction ratio of 8.4. The oxidant-fuel ratio was maintained around 5.0 with a characteristic length of 95 inches (2.41 m).

For comparison with experimental data, boundaries were generated on the analog computer using the double dead-time model and calculated values of delay. Experimental and computer data agreed with regard to the observed frequencies (both higher and lower ranges were observed with each configuration) and the boundary shape. (The reversal in slope was observed.) Discrepancies in boundary location (injector pressure drops required for stability) were attributed to a high combustion noise level.

INTRODUCTION

Low frequency combustion instabilities in liquid propellant rocket engines, commonly referred to as chugging, have been the subject of many analyses during the past two decades. The purpose of this investigation was to verify, experimentally, the chugging model advanced in reference 1. A comparison of the proposed double dead-time model and the commonly used single-delay model is given in figure 1. For the single-delay model, the injector flow rates are acted upon by a single delay, usually assumed to be made up of the governing vaporization time, mixing, and reaction times. For an oxidizer-vaporization limited system, this approach would be valid for the case of high fuel injector pressure drop. Under these conditions, fuel flow rate would be relatively constant during chugging, approximating the monopropellant case. To analyze chugging over a wide range of operating conditions and especially when one of the propellants is introduced as a gas at low pressures, the single-delay treatment will not suffice. The double dead-time model considers each propellant to be acted upon by a discrete time delay between injection and burning in the combustion chamber.

Figure 2 shows typical stability boundaries for both models, plotted as ratios of injector pressure drop to chamber pressure ($\Delta P/P$). All symbols are defined in appendix A. Regions above and to the right of the boundaries correspond to stable operation. For the case shown, the fuel is introduced as a gas with no vaporization time ($\tau_{v_f} = 0$). The single-delay boundary has the usual hyperbolic shape with the entire boundary corresponding to one chugging frequency. The double dead-time boundary has several distinctive characteristics. As the fuel $\Delta P/P$ is increased, the chugging frequency approaches a value (160 Hz) determined by the total oxidizer delay (2.75 msec) and the gas residence time. As the oxidizer $\Delta P/P$ is increased, the frequency approaches a value of about 360 hertz, determined by the total fuel delay (1.0 msec) and the gas residence time. The boundary is made up of two portions, each corresponding to a different range of chugging frequencies. Multi-mode oscillations have been observed and reported in reference 2. The lower frequency portion of the boundary has a characteristic reversal in slope indicating the possibility of stabilizing an engine by decreasing the fuel injector $\Delta P/P$ over a limited range. Such behavior has been observed and reported in reference 3.

The analysis of the bipropellant system considered in reference 1 was simplified by assuming constant injector cavity pressures (decoupled feed system). The system equations were linearized by assuming small perturbations in the system variables about steady-state operating values. Efforts were made to achieve these conditions during the experiments reported herein.

Experiments were conducted in the Rocket Combustion Laboratory at the NASA-Lewis Research Center. A 2-inch (5.08-cm) diameter rocket engine was run at nominal

chamber pressures of 650 and 300 pounds per square inch (4.48×10^6 and 2.07×10^6 N/m^2) absolute. The propellants were gaseous hydrogen at room temperature and liquid oxygen (LOX) at 140° R (77.8° K). The oxidizer-fuel mixture ratio was maintained around 5.0 with a total propellant mass flow rate of about 0.7 pound per second (0.317 kg/sec). Transitions from stable to unstable operation were accomplished by varying the injector geometries while maintaining the primary system variables (chamber pressure, flow rates) constant. Stability boundaries were determined for both configurations and compared with boundaries established on the analog computer using the double dead-time model.

APPARATUS

The flow system is shown schematically in figure 3. Pressure-regulated propellants, at ambient temperatures, were supplied to the system from storage bottles. The gaseous oxygen was liquefied in a liquid nitrogen bath. Valve and ignition sequencing was controlled by a preset electric timer. The chronology of ignition was as follows: (1) spark plug ignition and hydrogen bleed flow, (2) main oxidizer flow, and (3) main hydrogen flow. Relative timing between events was adjusted to give a smooth start.

Injector

A cut-away drawing of the injector is shown in figure 4. To conform with the model assumed in reference 1, it was necessary to maintain constant injector cavity pressures. That is, the pressure perturbations induced in the injector cavities during chugging had to be sufficiently attenuated. This attenuation was accomplished on the hydrogen side by adding a large volume (300 in.^{3}; 4.92×10^{-3} m^3) immediately upstream of the hydrogen injector manifold (see fig. 3). This method was not practical for the oxygen side, however, due to the high bulk modulus of liquid oxygen. Attenuation of the oxygen injector perturbations was provided by a thin (0.063 in.; 0.16 cm) inconel diaphragm (A). It was not possible to design a diaphragm with sufficient flexibility and yet sufficient strength to contain full manifold pressure. Therefore, most of the manifold pressure was balanced by gas pressure in volume (B). Volume (B) was pressurized, prior to running, to the anticipated manifold pressure minus about 15 psi (1.04×10^5 N/m^2). The thick perforated plate (C) supported the diaphragm against this preload. Careful design was required to insure that the diaphragm compliance would not couple with the inertance of the holes in plate (C) to produce a resonance in the frequency range of interest (30 to 300 Hz).

The hydrogen injector pressure drop was manipulated by changing the thickness (hence, porosity) of the transpiration-cooled faceplate (D). Thicknesses ranging from 0.125 to 0.250 inch (0.318 to 0.635 cm) were used to give the desired range of injector pressure drops.

The orifice plate (E) was used to vary the oxygen injector pressure drop. Flow diameters from 0.076 to 0.1285 inch (0.193 to 0.326 cm) were used. Minimum pressure drop was achieved with no orifice in the system. The injection tube (F) was made about ten diameters long in an attempt to maintain constant liquid jet properties at the chamber entrance.

Engine

An uncooled combustion chamber was used. Chamber wall thickness was 1.0 inch (2.54 cm). The inside diameter was 2.0 inches (5.08 cm) and the length was variable from 2.1 to 12.5 inches (5.33 to 31.8 cm). By changing chamber length, gas residence time (for stability studies) and burning length (for performance studies) could be evaluated.

With constant flow rates, chamber pressure was varied by changing the throat diameter of the water-cooled exhaust nozzle. Data were taken with throat diameters of 0.487 and 0.689 inch (1.24 and 1.75 cm), yielding nominal chamber pressures of 650 and 300 psia (4.48×10^6 and 2.07×10^6 N/m^2), respectively.

Instrumentation

The LOX flow rate was measured by means of a turbine-type flowmeter located in the nitrogen bath (see fig. 3). The gaseous hydrogen flow rate was measured with a critical flow venturi, located between the hydrogen fire valve and the 300 cubic inches (4.92×10^{-3} m^3) accumulator. Steady-state pressures were measured with strain gauge type transducers. Dynamic pressure measurements were made in the chamber and both injector cavities using piezoelectric transducers. The frequency responses of all dynamic pressure transducers were flat well beyond the frequency limit of this study (300 Hz). Output signals from all steady-state instrumentation were displayed on electrically-clamped meters. All transducer outputs were recorded on oscillograph paper. In addition, the output signal from the dynamic chamber pressure transducer was recorded on an FM tape recorder. The recorded signal was played back through a frequency analyzer, consisting of 30 filters with bandwidths of 1/3 octave and center fre-

quencies ranging from 40 to 31 500 hertz. Maximum steepness of the filter frequency characteristic was 120 decibels per octave.

PROCEDURE

Cold Flow Tests

Cold flow tests were conducted prior to the taking of stability data. With no hydrogen flow and the LOX diaphragm supported by high gas pressure, oxygen was flowed through the injector. LOX injector pressure drop against LOX flow rate is plotted in figure 5 for orifice diameters between 0.076 and 0.1275 inch (0.193 and 0.326 cm). As expected, pressure drop was proportional to the square of flowrate for a given orifice diameter.

With no LOX flow, room temperature hydrogen was exhausted through the fuel injector to the atmosphere. Faceplate thicknesses of 0.141 and 0.175 inch (0.358 and 0.444 cm) were run. Due to the compressibility of the hydrogen, flow through the faceplate is a function both pressure drop and downstream conditions. Assuming that (1) hydrogen temperature remains constant, and (2) pressure is distributed linearly through the faceplate, hydrogen flow rate can be calculated as follows:

$$\dot{w}_f = (C_d A)_R \left(2 g_c \rho_{f,av} \Delta P_{If}\right)^{1/2}$$

$$= (C_d A)_R \left(\frac{2 g_c}{R_f T_f}\right)^{1/2} \left(P_{f,av} \Delta P_{If}\right)^{1/2}$$

$$= K_R \left[(P_{If} - P_c)(P_{If} + P_c)\right]^{1/2} \qquad (1)$$

where

g_c force-mass conversion factor, 396 $(lb_m)(in.)/(lb_f)(sec^2)$; 1 $(kg)(m)/(N)(sec^2)$

$\dot{w}_f$ hydrogen mass flow rate through the Rigimesh faceplate, lb_m/sec; kg/sec

K_R faceplate coefficient (function of thickness), $(lb_m)(in.^2)/(sec)(lb_f)$; $(kg)(m^2)/(sec)(N)$

P_{If} fuel injector pressure, $lb_f/in.^2$; N/m^2

P_c chamber pressure, $lb_f/in.^2$; N/m^2

Figure 6 contains a plot of hydrogen flow rate against the quantity $\left[(P_{If} - P_c)(P_{If} + P_c)\right]^{1/2}$ for room temperature hydrogen exhausted to the atmosphere through specified faceplate thicknesses. The linearity of these plots and equation (1) permit computation of expected injector pressure drops for selected faceplate thicknesses and chamber pressures of 650 and 300 psia (4.48×10^6 and 2.07×10^6 N/m^2).

Figure 7 contains resultant information for room temperature hydrogen flowing at 0.11 pound per second (0.0499 kg/sec). Also shown are actual data points obtained during the hot run phase of the program.

System Definition

In an attempt to reduce the number of variables governing the vaporization process, it was decided to maintain constant LOX flow rate (hence, injection velocity), mixture ratio, and characteristic length, L* while running at each of the two throat sizes. With a throat diameter of 0.487 inch (1.24 cm), a chamber length of 4.1 inches (10.4 cm) was selected. This configuration yields an L* of 91.0 inches (2.31 m) and will be referred to as configuration A. With this configuration, a LOX flow rate of 0.55 pound per second (0.249 kg/sec) was required to reach a steady-state chamber pressure of 650 psia (4.48×10^6 N/m^2) at a nominal mixture ratio of 5.0.

With the available chamber lengths and a throat diameter of 0.689 inch (1.75 cm), the closest L* that could be run was 95.5 inches (2.43 m) with a chamber length of 9.85 inches (25.0 m). Running this configuration at a LOX flow rate of 0.55 pound per second (0.249 kg/sec) and a mixture ratio of 5.0 resulted in a nominal chamber pressure of 300 psia (2.07×10^6 N/m^2). This configuration will be referred to as configuation B. Further description of both configurations may be found in table I.

Stability Investigation

For both configurations, orifice diameters and faceplate thicknesses were selected using figures 5 and 7, respectively, to give a range of injector pressure drops from 0.05 $\overline{P}_c$ to 1.0 $\overline{P}_c$. In the case of the LOX injector, however, a minimum of about 50 psi (3.45×10^5 N/m^2) could be obtained at the prescribed flow rate by removing the orifice.

Since system operation was open-loop, it was necessary to iterate to the desired steady-state operating conditions. For a given system configuration, initial tank pressures were selected and set. With the ignition sequence controlled by the electric timer, the engine was fired for approximately 4 seconds. Timing was adjusted to give

slightly more than 2 seconds of steady-state operation. Adjustments were made in the tank pressures so as to decrease the errors between measured and desired flow rates. In general, LOX and fuel mass flow rates were held within 10 percent of 0.55 and 0.11 pound per second (0.249 and 0.0499 kg/sec), respectively. Destabilization of the engine was accomplished by increasing the LOX orifice size while maintaining faceplate thickness and the other system variables constant.

The electric timer was also used to gate the output of the dynamic chamber pressure transducer to the tape recorder. The gating circuit also provided 2 seconds of reference ground both before and after the steady-state data. Figure 8 shows a typical start transient, recorded on oscillograph paper with the timer events noted.

Performance Investigation

A model describing the vaporization process for a single droplet has been developed by Priem and Heidmann (ref. 4). For the case of a completely vaporized fuel, combustion efficiency is completely defined by the percentage of the oxidizer mass vaporized within the chamber. Heidmann and Wieber (ref. 5) have been able to correlate frequency response data obtained with this model with that obtained using a pure delay model with delay equal to the time required to vaporize 50 percent of the mass of an injected droplet. From these results, it follows that (1) at a chamber pressure of 300 psia (2.07×10^6 N/m^2), (2) a mixture ratio of 5.0, and (3) with a chamber length yielding a combustion efficiency of 62 percent, 50 percent of the oxidizer mass will be vaporized within the chamber. To determine this length, of the oxidizer mass will be vaporized within the chamber. To determine this length, a faceplate thickness of 0.165 inch (0.419 cm) and an orifice diameter of 0.098 inch (0.249 cm) were selected to give stable operation with a throat diameter of 0.689 inch (1.75 cm). Chamber lengths, ranging from 2.1 to 12.5 inches (5.33 to 31.8 cm) were run with tank pressures adjusted to give a chamber pressure of 300 psia (2.07×10^6 N/m^2) and a mixture ratio of 5.0.

Data Analysis

Frequency analysis of the recorded chamber pressure data showed that, in all cases, the chamber pressure oscillation could be considered as having two frequency components. Using the frequency analyzer filters, the two filtered signals for each run were rerecorded on oscillograph paper for further analysis. Figure 9 shows the envelope of a typical filtered signal observed during chugging. Due to the observed randomness in chamber pressure amplitude, a stability criterion based on a time-average over a set

portion of the run was selected. Any oscillation having an rms amplitude exceeding 10 percent of the mean chamber pressure for 1 second was considered unstable.

A total of 76 experimental runs was made with configuration A and 53 with configuration B. It was felt that some realistic criteria should be applied to the data to separate "good" from "bad" data points. The following criteria were selected: (1) orifice repeatability, (2) faceplate repeatability, and (3) performance repeatability. Since cold-flow tests established the oxygen flow through the orifice as having a square law characteristic and since a constant density fluid was assumed, the following parameter was selected as a measure of orifice repeatability:

$$C_{d_o}(\rho_o)^{1/2} = \dot{w}_o A_o^{-1}\ 2g_c(P_{Io} - P_c)^{-1/2} \tag{2}$$

Faceplate repeatability (for a given thickness) was based on the parameter K_R^{-1} as defined in equation (1). From observing the system behavior over a wide range of operating conditions, combustion efficiency was found to be a function of the stability of the system. For a particular stability classification (lower or higher frequency, stable or unstable), combustion efficiency was selected as a measure of system repeatability. The parameters $C_{d_o}(\rho_o)^{1/2}$, K_R^{-1}, and η_{c*} were assumed to be normally distributed about some mean value with an allowable spread of ± 1.5 times the computed standard deviation. Based on the analysis, a total of 18 runs with configuration A and 10 runs with configuration B were judged to be "bad". Pertinent data for the acceptable runs are listed in tables II and III. A summary of the data analysis is given in appendix B. System gains (injector $\Delta P/P$) for both configurations were normalized to $O/F = 5.0$ conditions as described in appendix C.

RESULTS AND DISCUSSION

Chugging Results

Figure 10(a) shows the 58 acceptable runs for configuration A plotted on a $\Delta P/P$ map. A boundary, based on the 10 percent rms criterion, has been drawn between those points classified as stable or unstable. Corresponding chugging frequencies, for points near the boundary, have been noted on the figure. Oscillations in both the 70 and 170 hertz ranges were observed. Note the characteristic reversal in slope of the lower frequency portion of the boundary. At an oxidizer $\Delta P/P$ of 0.4, a reduction in the fuel $\Delta P/P$ from 0.4 to 0.2 resulted in a stabilization of the engine.

Figure 10(b) shows the 43 acceptable runs for configuration B. A boundary has been drawn based on the 10 percent rms criterion. Unlike the high pressure case, however, the boundary has an irregular shape. A bending back of the boundary takes place at both extremes of fuel injector pressure drop. Since control of fuel velocity was sacrificed for ease of changing the injector pressure drop, fuel velocity is not constant over the range of fuel injector $\Delta P/P$'s. The resulting effect on oxidizer drop size and vaporization rate may be the cause of the irregular boundary shape. Another possible cause might be coupling of the feed system in spite of the efforts made to prevent such an occurrence. Chugging frequencies in both the 40 and 100 hertz ranges were observed, together with the reversal in slope of the low frequency portion of the boundary.

Performance Results

Figure 11 contains a plot of combustion efficiency against chamber length for a chamber pressure of 300 psia (2.07×10^6 N/m^2). Results obtained in reference 6 substantiate the low performance obtained with this injector. A combustion efficiency of 75 percent would be expected with a chamber pressure of 300 psia (2.07×10^6 N/m^2), chamber diameter of 2.0 inches (5.08 cm), chamber length of 8.0 inches (20.3 cm), throat diameter of 0.75 inch (1.90 cm), mixture ratio of 5.0, and a single-element, concentric tube injector. A slightly lower efficiency (71.1 percent) was obtained with configuration B which approximates these conditions with the single-element, transpiration-cooled injector.

Based on the vaporization model of Priem and Heidmann, the length required to vaporize 50 percent of the oxidizer droplet mass ($\eta_{c*} = 0.616$) is 5.5 inches (14.0 cm). If one assumes that the average droplet velocity over this length is equal to the injection velocity (ref. 4), the vaporization time can be computed from $l_{50}v_j^{-1} = 7.48$ milliseconds for configuration B. This result, when applied to the vaporization model of Priem and Heidmann, yields a vaporization time of 4.62 milliseconds for configuration A.

Values of mixing and reaction times were calculated for both configurations using the calculated values of vaporization time and the total oxidizer delays required to satisfy the phase requirement for neutral stability at high values of fuel $\Delta P/P$ and the observed chugging frequencies. Mixing times of 3.8 and 2.1 millisecond were determined for configurations A and B, respectively.

Computer Simulation

For comparison with experimental data, stability boundaries were generated using an analog computer simulation of the double dead-time model. The Analog Computer

Facility of the Lewis Research Center was used. Boundaries were obtained at chamber pressures of 650 and 300 psia (4.48×10^6 and 2.07×10^6 N/m^2) with a LOX flow rate of 0.55 pound per second (0.249 kg/sec) and a mixture ratio of 5.0. The nonlinear differential equations presented in reference 1 were programmed on the computer, using a 1:1 time scale. A variable diode-function generator was used to represent the C^*_{th} - O/F relation. Two variable delay lines were used to represent the total oxidizer and fuel delays. A one lump representation of the oxygen feed system (line, fire valve) was developed from measured line dimensions and valve calibrations. A summary of the equations, represented on the computer, is given in appendix D.

A stability boundary was obtained on the computer by (1) selecting values for vaporization, mixing and gas residence time, (2) setting the value of K_R to give the desired fuel injector pressure drop, (3) continuously varying K_o (LOX injector pressure drop) while adjusting tank pressure to maintain flow rate constant, (4) combining the chamber pressure signal with the output of a sinusoidal oscillator to produce a lissajous figure on an oscilloscope screen, (5) adjusting the oscillator frequency until a stable pattern appeared on the screen (the corresponding frequency being equal to the chugging frequency), (6) repeating the process at selected values of K_R to form a boundary, (7) readjusting the delays and/or gas residence time to match the experimentally observed chugging frequencies over the entire boundary.

Table IV gives the required values of delay together with the initial calculated values. LOX vaporization times were within 7 percent of those calculated using the vaporization model of Priem and Heidmann. All delay values were within 10 percent of the initial calculated values.

In an attempt to match the randomness of the chamber pressure oscillations, the physical system was simulated with white noise superimposed on the products of combustion. The presence of a high combustion noise level could be attributed to the coarse injection pattern. The noise generator output was adjusted to give approximately 7 percent stable oscillations in chamber pressure with high injector pressure drops. This approximated the observed experimental noise level. Figure 12 gives a comparison between experimental and noise-induced chamber pressure oscillations at a fixed fuel injector pressure drop with variable LOX injector pressure drop. The 0.25 level of oxidizer $\Delta P/P$ corresponds to the inherent stability boundary (no disturbance). It is seen that the transition from stable to unstable operation is a gradual one with amplitudes of oscillation ranging from 7 to 36 percent of the mean chamber pressure. Using the 10 percent rms criterion for stability, a shift occurs in the apparent boundary position from 0.25 to 0.40.

Figure 13 shows the sensitivity of the entire computer boundary to the input noise level for configuration A. It is seen that the introduction of noise into the system results in a shift in the entire boundary for a fixed stability criterion. A slight increase in the

boundary frequencies was noted with increased noise levels.

Figure 14(a) gives a comparison between the experimental boundary for configuration A and the computer boundary obtained with the 7 percent noise level. Chugging frequencies between 63 and 85 hertz and between 147 and 210 hertz were observed both experimentally and on the computer. In reference 3, a ratio of 2.7 between higher and lower frequencies has been noted during multi-mode oscillations. Data for that study were taken at high values of fuel $\Delta P/P$ so as to approximate a monopropellant system. An average ratio of 2.5 was observed experimentally with configuration A at values of $\Delta P_{lf}/P_c$ above 0.5. Excellent agreement between the experimental and computer boundary shapes was obtained for configuration A. As predicted by the double dead-time model, a reversal in slope occurs for the lower frequency portion of the boundary with an intersection with the higher frequency portion of the boundary occurring at a fuel $\Delta P/P$ around 0.15. Deviations between the boundaries at low fuel $\Delta P/P$'s may be due to the effect of fuel velocity on the oxidizer drop size and vaporization rate. The possibility also exists that backflow through the fuel injector occurs at low values of fuel $\Delta P/P$ during chugging with a stabilizing effect. Excellent agreement in boundary position was obtained with the 7 percent noise level.

Figure 14(b) gives a comparison between the experimental boundary for configuration B and the computer boundary obtained with the 7 percent noise level. Chugging frequencies between 39 and 46 hertz and between 99 and 112 hertz were observed. An average frequency ratio of 2.5 was observed at values of fuel $\Delta P/P$ above 0.5. The bending back of the higher frequency portion of the experimental boundary may be attributed to velocity effects or possible coupling of the feed system. A higher percent noise level would be required to match the boundary position indicating that the absolute noise level is a function of the injector configuration and not chamber pressure. A 15 percent noise level with configuration B would be equivalent to the 7 percent noise level observed with configuration A. Both characteristics of the double dead-time model were exhibited by both boundaries however. A reversal in slope of the lower frequency portion of the boundary together with two ranges of frequency along the boundary were observed.

SUMMARY OF RESULTS

Stability limits were determined, experimentally, for a 2-inch (5.08-cm) diameter rocket engine. Liquid oxygen and gaseous hydrogen were the propellants. Boundaries were determined for two engine configurations: a chamber pressure of 650 psia (4.48×10^6 N/m^2), contraction ratio of 16.8, and a chamber pressure of 300 psia (2.07×10^6 N/m^2), contraction ratio of 8.4. The oxidizer-fuel mixture ratio was main-

tained at 5.0 with a characteristic length of about 95 inches (2.41 m). For comparison with experimental data, stability boundaries were generated on the analog computer using the chugging model proposed by the authors in reference 1 and values of combustion delay determined from an existing vaporization model. The results of this study can be summarized as follows:

1. The validity of the double dead-time model has been demonstrated. Both configurations investigated exhibited the characteristic behavior of the model. That is, more than one range of frequency along the stability boundary was observed together with a reversal in slope of the lower frequency portion of the boundary.

2. Values of LOX vaporization times required to match the observed chugging frequencies were within 7 percent of those predicted by Priem and Heidmann.

3. Mixing and reaction times must be inferred from the calculated values of vaporization time and the observed chugging frequencies.

4. The choice of a single element injector configuration resulted in a high combustion noise level requiring the selection of an arbitrary time-average criterion for stability. Boundary positions were matched using the model and an experimentally determined 7 percent noise level.

Lewis Research Center,
National Aeronautics and Space Administration,
Cleveland, Ohio, January 23, 1968,
128-31-01-13-22.

APPENDIX A

SYMBOLS

A	cross-sectional area, in^2; m^2
C_d	orifice coefficient
C^*_{th}	theoretical characteristic velocity, in/sec; m/sec
d	cross-sectional diameter, in; m
f	experimentally-observed frequency, Hz
f'	computer-observed frequency, Hz
G	system gain
g_c	force-mass-conversion factor, 386 $(lb_m)(in.)/(lb_f)(sec^2)$; 1 $(kg)(m)/(N)(sec^2)$
K_o	oxidizer orifice coefficient, $(lb_m)(in)/(sec)(lb_f)^{1/2}$; $(kg)(m)/(sec)(N)^{1/2}$
K_R	fuel faceplate coefficient, $(lb_m)(in.^2)/(lb_f)(sec)$; $(kg)(m^2)/(N)(sec)$
l	length, in.; m
L^*	characteristic length, in.; cm
N	number of data points in specific sample
n	white noise signal, lb_m/sec; kg/sec
O/F	mixture ratio
P	static pressure, lb_f/in^2
$\dot{P}$	time-derivative of pressure, $lb_f/(in.^2)(sec)$; $N/(m^2)(sec)$
R	gas constant, $in./^oR$; $m/^oK$
$\mathcal{R}$	mixture ratio notation O/F
rms	root-mean-square amplitude of chamber pressure oscillation, $lb_f/in.^2$; N/m^2
S_x	estimated standard deviation of an assumed random parameter x, units of x
s	Laplace operator, sec^{-1}
T	temperature, ^oR; ^oK
t	time, sec
t_R	fuel faceplate thickness, in; m
V	volume, $in.^3$; m^3
v	velocity, in/sec; m/sec
$\dot{w}$	mass flow rate, lb_m/sec; kg/sec
$\overline{\dot{w}}_f$	fuel mass flow rate, $K_f\sqrt{\overline{P}^2_{If} - \overline{P}^2_c}$, lb_m/sec; kg/sec
$\overline{\dot{w}}_o$	oxidizer mass flow rate, $K_o\sqrt{\overline{P}_{Io} - \overline{P}_c}$, lb_m/sec; kg/sec
$\ddot{w}$	time derivative of mass flow rate, lb_m/sec^2; kg/sec^2
x	general system parameter x, units of x
$\bar{x}$	mean value of parameter x, units of x
α	variable mixture ratio gain factor

ΔP	pressure drop (assumed positive), $lb_f/in.^2$; N/m^2
γ	specific heat ratio of combustion products
η_{c^*}	combustion efficiency
ρ	fluid mass density, $lb_m/in.^3$; kg/m^3
τ	time delay, sec
θ_g	theoretical gas residence time, sec

Subscripts:

av	average
b	products of combustion
c	combustion chamber
f	fuel
i	i^{th} measurements of variable x (i = 1, 2, . . . N)
If	fuel injector
Io	oxidizer injector
j	oxidizer jet
LO	oxidizer line
m	mixing
n	exhaust nozzle
o	oxidizer
R	transpiration-cooled faceplate
t	exhaust nozzle throat
TO	oxidizer tank
vf	fuel vaporization
vo	oxidizer vaporization
50	50-percent mass vaporized

APPENDIX B

DATA ANALYSIS

x = selected parameter

$x_i = i^{th}$ measurement of parameter ($i = 1, 2, 3, \ldots N$)

N = number of measurements

$\bar{x}$ = mean value of parameter $= \dfrac{\sum_{i=1}^{N} x_i}{N}$

S_x = estimated value of standard deviation of parameter

$$= \left[\frac{\sum_{i=1}^{N} (x_i - \bar{x})^2}{(N - 1)}\right]^{1/2}$$

Configuration A Analysis

1. Orifice repeatability

$$x = C_d(\rho_o)^{1/2} = \dot{w}_o A_o^{-1} \left[2g_c(P_{Io} - P_c)\right]^{-1/2}$$

$N = 76$

$$\bar{x} = 0.164 \frac{lb_m^{1/2}}{in.^{3/2}}; \qquad 27.3 \frac{kg^{1/2}}{m^{3/2}}$$

$$S_x = 0.0212 \frac{lb_m^{1/2}}{in.^{3/2}}; \qquad 3.53 \frac{kg^{1/2}}{m^{3/2}}$$

number of excluded points = 7.

2. Faceplate repeatability

$$x = \dot{w}_f^{-1} \left(P_{If}^2 - P_c^2\right)^{1/2} = K_R^{-1}$$

Thickness		N	$10^{-2}\,\bar{x}$		$10^{-2}\,S_x$		Number of excluded points
in.	cm		$\frac{(lb_f)(sec)}{(lb_m)(in.^2)}$	$\frac{(N)(sec)}{(kg)(m^2)}$	$\frac{(lb_f)(sec)}{(lb_m)(in.^2)}$	$\frac{(N)(sec)}{(kg)(m^2)}$	
0.125	0.318	6	97.6	14.8	7.80	1.19	0
.137	.348	5	88.8	13.5	3.89	.591	0
.141	.358	9	67.8	10.3	2.99	.454	0
.148	.376	9	47.1	7.16	1.92	.292	2
.154	.391	9	37.2	5.65	1.42	.216	0
.158	.401	9	34.1	5.18	2.17	.330	0
.165	.419	9	25.4	3.86	1.04	.158	1
.175	.444	7	21.0	3.19	1.81	.275	0
.185	.470	6	17.0	2.58	1.82	.277	0

3. Performance repeatability

$$x = \eta_{c*} = A_t g_c P_c \left(\dot{w}_o + \dot{w}_f\right)^{-1} C_{th}^{*-1}$$

Lower frequency classification	Higher frequency classification	N	$\bar{x}$	S_x	Number of excluded points
Stable	Stable	45	0.739	0.0515	6
Unstable	Unstable	1	.675	------	0
Stable	Unstable	4	.628	.0660	0
Unstable	Stable	16	.691	.0626	2

Configuration A total excluded points = 18.

Configuration B Analysis

1. Orifice repeatability

$$x = C_d(\rho_o)^{1/2} = \dot{w}_o A_o^{-1} \; 2g_c \left[(P_{Io} - P_c)\right]^{-1/2}$$

N = 53

$$\bar{x} = 0.154 \left(lb_m^{1/2}\right)\left(in.^{-3/2}\right); \quad 25.6 \left(kg^{1/2}\right)\left(m^{-3/2}\right)$$

$$S_x = 0.0214 \left(lb_m^{1/2}\right)\left(in.^{-3/2}\right); \quad 3.56 \left(kg^{1/2}\right)\left(m^{-3/2}\right)$$

number of excluded points = 5.

2. Faceplate repeatability

$$x = \dot{w}_f^{-1} \left(P_{If}^2 - P_c^2\right)^{1/2} = K_R^{-1}$$

Thickness		N	$10^{-2}\,\bar{x}$		$10^{-2}\,S_x$		Number of excluded points
in.	cm		$\frac{(lb_f)(sec)}{(lb_m)(in.^2)}$	$\frac{(N)(sec)}{(kg)(m^2)}$	$\frac{(lb_f)(sec)}{(lb_m)(in.^2)}$	$\frac{(N)(sec)}{(kg)(m^2)}$	
0.141	0.358	6	63.0	9.58	0.693	0.105	0
.148	.376	7	42.3	6.43	1.87	.284	1
.154	.391	5	35.3	5.37	.357	.0543	0
.158	.401	5	29.7	4.51	.430	.0654	0
.165	.419	6	22.8	3.47	.380	.0578	0
.175	.444	6	18.5	2.81	.590	.0897	0
.185	.470	4	14.9	2.26	1.05	.160	0
.200	.508	2	11.0	1.67	.424	.0644	0
.217	.551	3	9.67	1.47	.141	.0214	0
.250	.635	4	7.80	1.19	.687	.104	0

3. Performance repeatability

$$x = \eta_{c*} = A_t g_c P_c \left(\dot{w}_o + \dot{w}_f\right)^{-1} C_{th}^{*-1}$$

Lower frequency classification	Higher frequency classification	N	$\bar{x}$	S_x	Number of excluded points
Stable	Stable	20	0.711	0.0391	2
Unstable	Unstable	10	.689	.0286	1
Stable	Unstable	11	.690	.0302	0
Unstable	Stable	6	.693	.0347	1

Configuration B total excluded points = 10.

APPENDIX C

NORMALIZATION OF ENGINE GAINS FOR OFF-MIXTURE RATIO CONDITIONS

From the linearization of the system equations as described in reference 1, the characteristic equation for the closed-loop system can be written as:

$$0 = 1 + \frac{e^{-\tau_m s}}{(\theta_g S + 1)} \left(G_o \, e^{-\tau_{vo} s} + G_f \right)$$

where

$$G_o = \frac{\partial P_c}{\partial \dot{w}_c} \frac{d\dot{w}_o}{d\,\Delta P_{Io}} = \frac{P_c}{(\dot{w}_o + \dot{w}_f)} \left[1 + \frac{(\mathcal{R} + 1)}{C^*_{th}} \frac{\partial C^*_{th}}{\partial \mathcal{R}} \frac{d\dot{w}_o}{d\,\Delta P_{Io}} \right]$$

$$G_f = \frac{\partial P_c}{\partial \dot{w}_f} \frac{d\dot{w}_f}{d\,\Delta P_{If}} = \frac{P_c}{(\dot{w}_o + \dot{w}_f)} \left[1 - \frac{\mathcal{R}(\mathcal{R} + 1)}{C^*_{th}} \frac{\partial C^*_{th}}{\partial \mathcal{R}} \frac{d\dot{w}_f}{d\,\Delta P_{If}} \right]$$

if $\dot{w}_o$ is proportional to $\left(\Delta P_{Io}\right)^{1/2}$; $\dot{w}_f$ is proportional to $\left(P_{If}^2 - P_c^2\right)^{1/2}$; P_{Io}, P_{If} nontime varying

$$\frac{d\,\dot{w}_o}{d\,\Delta P_{Io}} = \frac{\dot{w}_o}{2\,\Delta P_{Io}}$$

$$\frac{d\,\dot{w}_f}{d\,\Delta P_{If}} = \frac{\dot{w}_f P_c}{\Delta P_{If}(\Delta P_{If} + 2P_c)}$$

Therefore,

$$G_o = \frac{\alpha_o}{2\,\frac{\Delta P_{Io}}{P_c}}$$

where

$$\alpha_o = \frac{\mathcal{R}}{(\mathcal{R}+1)} + \frac{\mathcal{R}}{C^*_{th}} \frac{\partial C^*_{th}}{\partial \mathcal{R}}$$

$$G_f = \frac{\alpha_f}{2 \frac{\Delta P_{If}}{P_c} \left(\frac{\Delta P_{If}}{2P_c} + 1 \right)}$$

where

$$\alpha_f = \frac{1}{(\mathcal{R}+1)} - \frac{\mathcal{R}}{C^*_{th}} \frac{\partial C^*_{th}}{\partial \mathcal{R}}$$

For the same system gains at off-mixture ratio conditions, the $\Delta P/P$'s can be normalized to $\mathcal{R} = 5.0$ conditions by:

$$\left(\frac{\Delta P_{Io}}{P_c} \right)_{\mathcal{R}=5} = \frac{\alpha_{o\,\mathcal{R}=5}}{\alpha_{o\,\mathcal{R}}} \left(\frac{\Delta P_{Io}}{P_c} \right)_{\mathcal{R}}$$

$$\frac{\Delta P_{If}}{P_c} \left(1 + \frac{\Delta P_{If}}{2P_c} \right)_{\mathcal{R}=5} = \frac{\alpha_{f\,\mathcal{R}=5}}{\alpha_{f\,\mathcal{R}}} \frac{\Delta P_{If}}{P_c} \left(1 + \frac{\Delta P_{If}}{2P_c} \right)_{\mathcal{R}}$$

APPENDIX D

SUMMARY OF EQUATIONS REPRESENTED ON THE ANALOG COMPUTER

1. Pressures in $lb_f/in.^2$; flow rates in lb_m/sec

$$P_{TO} - P_{LO} = 155\,\dot{w}_{TO}^2 + 5.90\,\ddot{w}_{TO}$$

$$P_{LO} = 4.01\times10^6 \int (\dot{w}_{TO} - \dot{w}_{LO})\,dt$$

$$P_{LO} - P_{Io} = 400\,\dot{w}_{LO}^2 + 9.36\,\ddot{w}_{LO}$$

$$P_{Io} = 1.37\times10^3 \int (\dot{w}_{LO} - \dot{w}_{Io})\,dt$$

$$P_{Io} - P_c = K_o\dot{w}_{Io}^2 + 0.214\,\ddot{w}_{Io}$$

$$\theta_g\dot{P}_c + P_c = \frac{C_{th}^*}{A_t g_c}\left[w_{Io}(t - \tau_{vo} - \tau_m) + \dot{w}_{If}(t - \tau_m) + n(t)\right]$$

$$\dot{w}_{If} = K_R\left(P_{If}^2 - P_c^2\right)^{1/2}$$

$$O/F = \frac{\dot{w}_{Io}(t - \tau_{vo} - \tau_m)}{\dot{w}_{If}(t - \tau_m)}$$

2. Pressures in N/m^2; flow rates in kg/sec

$$P_{TO} - P_{LO} = 5.19\times10^6\,\dot{w}_{TO}^2 + 8.97\times10^4\,\ddot{w}_{TO}$$

$$P_{LO} = 6.10\times10^{10} \int (\dot{w}_{TO} - \dot{w}_{LO})\,dt$$

$$P_{LO} - P_{Io} = 1.67\times10^7\,\dot{w}_{LO}^2 + 1.42\times10^5\,\ddot{w}_{LO}$$

$$P_{Io} = 2.08\times10^7 \int (\dot{w}_{LO} - \dot{w}_{Io})\,dt$$

$$P_{Io} - P_c = K_o\dot{w}_{Io}^2 + 3.25\times10^3\,\ddot{w}_{Io}$$

REFERENCES

1. Wenzel, Leon M.; and Szuch, John R.: Analysis of Chugging in Liquid-Bipropellant Rocket Engines Using Propellants with Different Vaporization Rates. NASA TN D-3080, 1965.

2. Heidmann, Marcus F.: Oxygen-Jet Behavior During Combustion Instability in a Two-Dimensional Combustor. NASA TN D-2725, 1965.

3. Anon.: J-2 Program Quarterly Progress Report for Period Ending February 28, 1962. Rep. No. R-2600-6 (NASA CR-63323), Rocketdyne Div., North American Aviation, Mar. 28, 1962, pp. 85, 137-140.

4. Priem, Richard J.; and Heidmann, Marcus F.: Propellant Vaporization as a Design Criterion for Rocket-Engine Combustion Chambers. NASA TR R-67, 1960.

5. Heidmann, Marcus F.; and Wieber, Paul R.: An Analysis of the Frequency Response Characteristics of Propellant Vaporization. Paper presented at the AIAA Second Propulsion Joint Specialist Conference, Colorado Springs, Colorado, June 13-17, 1966.

6. Heidmann, Marcus F.; and Baker, Louis, Jr.: Combustor Performance with Various Hydrogen-Oxygen Injection Methods in a 200-Pound-Thrust Rocket Engine. NACA RM E58E21, 1958.

TABLE I. - DESCRIPTION OF ENGINE CONFIGURATIONS STUDIED

	Configuration	
	A	B
Chamber diameter, d_c, in.; cm	2.00; 5.08	2.00; 5.08
Throat diameter, d_t, in.; cm	0.487; 1.24	0.689; 1.75
Chamber length, ℓ_c, in.; cm	4.10; 10.4	9.85; 25.0
Characteristic length, L*, in.; m	91.0; 2.31	95.5; 2.43
Theoretical gas residence time, θ_g, at O/F = 5, msec	2.40	2.50
Nominal mixture ratio, O/F	5.00	5.00
Nominal chamber pressure, P_c, $lb_f/in.^2$; N/m^2	650; 4.48×10^6	300; 2.07×10^6
Nominal LOX mass-flow rate, $\dot{w}_o$, lb_m/sec; kg/sec	0.55; 0.249	0.55; 0.249

TABLE II. - CONFIGURATION A DATA

Run	Chamber pressure, P_c		Mixture ratio, $\mathcal{R}$	LOX flow rate, $\dot{w}_o$		Combustion efficiency, η_{c^*}	Fuel pressure-drop ratio, $\frac{\Delta P_{If}}{P_c}$	LOX pressure-drop ratio, $\frac{\Delta P_{Io}}{P_c}$	Lower frequency classification	Higher frequency classification	Observed lower frequency, Hz	Observed higher frequency, Hz	Fuel gain normalizing factor, $\frac{(\alpha_f)_{\mathcal{R}=5}}{(\alpha_o)_{\mathcal{R}}}$	LOX gain normalizing factor, $\frac{(\alpha_f)_{\mathcal{R}=5}}{(\alpha_o)_{\mathcal{R}}}$	Normalized fuel pressure-drop ratio, $\left(\frac{\Delta P_{If}}{P_c}\right)_{\mathcal{R}=5}$	Normalized LOX pressure-drop ratio, $\left(\frac{\Delta P_{Io}}{P_c}\right)_{\mathcal{R}=5}$
	$lb_f/in.^2$	N/m^2		lb_m/sec	kg/sec											
74	700	4.83×10^6	5.01	0.561	0.254	0.787	0.511	0.656	Stable	Stable	78	195	0.997	1.00	0.509	0.656
75	696	4.80	4.85	.558	.253	.778	.530	.567			78	195	1.06	.973	.562	.551
76	696	4.69	4.85	.567	.257	.748	.577	.478			77	195	1.06	.973	.612	.465
78	676	4.66	4.77	.573	.260	.732	.287	.942			70	205	1.08	.962	.310	.906
80	695	4.75	5.16	.583	.264	.760	.248	.576			70	190	.950	1.03	.236	.593
82	665	4.59	4.76	.538	.244	.766	.184	1.02			80	195	1.09	.960	.201	.979
83	695	4.75	5.00	.575	.261	.762	.159	.576			80	190	1.00	1.00	.159	.576
84	675	4.65	4.80	.567	.257	.740	.182	.622			85	195	1.08	.965	.197	.600
85	685	4.72	4.86	.579	.263	.739	.172	.472			80	205	1.05	.975	.181	.460
87	695	4.75	4.70	.555	.252	.773	.133	.834			84	165	1.12	.950	.149	.792
88	695	4.75	5.17	.585	.265	.758	.122	.522			83	194	.948	1.03	.116	.538
91	693	4.78	4.97	.591	.268	.737	.0820	.840			82	210	1.01	.995	.0828	.836
92	698	4.81	4.80	.585	.265	.752	.0850	.440			82	195	1.00	1.00	.0850	.440
94	680	4.69	5.04	.585	.265	.734	.0480	.831			--	---	.988	1.01	.0474	.839
96	655	4.52	5.04	.585	.265	.708	.0760	.386			80	200	.988	1.01	.0751	.390
98	717	4.94	5.43	.603	.273	.772	.0250	.726			--	---	.894	1.07	.0224	.777
100	640	4.41	4.85	.563	.255	.709	.0250	.430			79	200	1.06	.973	.0456	.418
108	675	4.65	5.01	.521	.236	.817	.711	1.02			63	162	.999	1.00	.0710	1.02
109	698	4.81	5.20	.557	.253	.801	.698	.532			78	195	.942	1.04	.0658	.553
111	675	4.65	5.01	.561	.254	.759	.756	.444			70	190	.998	1.00	.0754	.444
113	685	4.72	5.38	.597	.271	.742	.167	.960			78	155	.900	1.06	.150	1.02
114	662	4.56	4.71	.542	.246	.755	.196	.960			78	200	1.11	.951	.218	.654
115	665	4.59	5.13	.585	.265	.723	.196	.688			80	198	.959	1.03	.188	.480
116	655	4.52	4.88	.561	.254	.730	.214	.397			75	188	1.05	.980	.225	.389
117	617	4.25	4.81	.563	.255	.682	.240	.361			71	186	1.07	.967	.257	.349

119	687	4.74×10^6	5.01	0.567	0.257	0.764	0.266	0.594	Stable	Stable	72	200	0.997	1.00	0.265	0.594
123	645	4.45	5.30	.567	.257	.732	.081	1.08			68	165	.919	1.05	.0744	1.13
124	635	4.38	5.30	.595	.270	.687	.098	.677			78	195	.919	1.05	.0900	.711
125	592	4.08	5.06	.561	.254	.668	.102	.444			80	183	.981	1.01	.100	.448
126	600	4.14	4.83	.536	.243	.697	.112	.362			80	170	1.06	.970	.119	.351
127	565	3.90	4.73	.530	.240	.660	.115	.327			72	175	1.10	.955	.127	.312
130	705	4.86	5.16	.573	.260	.784	.121	.553			80	190	.950	1.03	.166	.570
131	655	4.52	5.01	.561	.254	.736	.166	.431			78	190	.997	1.00	.115	.431
135	695	4.75	5.14	.581	.263	.761	.446	.867			78	205	.956	1.03	.426	.893
136	680	4.69	5.04	.585	.265	.734	.480	.566			74	200	.988	1.01	.474	.572
142	618	4.26	4.81	.558	.253	.689	.080	.384			80	195	1.07	.967	.0856	.371
143	596	4.11	4.86	.549	.249	.678	.082	.384			82	195	1.05	.975	.0851	.374
144	597	4.12	5.01	.542	.246	.695	.080	.284			85	182	.997	1.00	.0798	.284
90	635	4.38	5.10	.597	.271	.675	.422	.207	Unstable	Unstable	78	150	.969	1.02	.431	.200
97	675	4.65	4.87	.585	.265	.721	.053	.218	Stable		78	198	1.05	.977	.0556	.213
128	515	3.55	4.88	.542	.246	.594	.136	.209			72	178	1.05	.980	.143	.205
145	535	3.69	4.91	.536	.243	.625	.094	.178			72	180	.905	.986	.0861	.176
148	487	3.36	4.96	.536	.243	.571	.078	.093			75	178	1.01	.994	.0788	.0924
71	630	4.34	4.81	.573	.260	.684	.893	.298	Unstable	Stable	68	202	1.07	.967	.955	.288
77	595	4.10	5.15	.618	.280	.613	.744	.324			67	205	.953	1.03	.709	.334
81	653	4.50	5.03	.610	.277	.676	.321	.406			75	210	.990	1.01	.318	.410
89	690	4.76	5.19	.610	.254	.785	.152	.435			78	153	.943	1.04	.143	.452
110	623	4.30	4.92	.585	.265	.667	.895	.396			68	200	1.03	.987	.922	.391
112	615	4.24	5.12	.558	.253	.700	.927	.390			68	200	.962	1.02	.892	.398
121	635	4.38	5.00	.585	.265	.684	.346	.394			70	190	1.00	1.00	.346	.394
132	598	----	5.04	.585	.265	.646	.209	.417			74	150	.988	1.01	.206	.421
133	575	----	4.94	.563	.255	.641	.226	.388			71	140	1.02	.990	.231	.884
134	535	----	5.01	.561	.254	.601	.214	.276			69	205	.998	1.00	.214	.276
137	650	----	5.16	.567	.257	.730	.523	.458			74	150	.950	1.03	.497	.472
138	615	----	4.77	.540	.245	.707	.573	.439			72	147	1.08	.962	.619	.422
139	595	----	5.00	.581	.263	.646	.613	.387			70	210	1.00	1.00	.613	.387

TABLE III. - CONFIGURATION B DATA

Run	Chamber pressure, P_c		Mixture ratio, $\mathcal{R}$	LOX flow rate, $\dot{w}_o$		Combustion efficiency, η_{c^*}	Fuel pressure-drop ratio, $\frac{\Delta P_{If}}{P_c}$	LOX pressure-drop ratio, $\frac{\Delta P_{Io}}{P_c}$	Lower frequency classification	Higher frequency classification	Observed lower frequency, Hz	Observed higher frequency, Hz	Fuel gain normalizing factor, $\frac{(\alpha_f)_{\mathcal{R}=5}}{(\alpha_o)_{\mathcal{R}}}$	LOX gain normalizing factor, $\frac{(\alpha_f)_{\mathcal{R}=5}}{(\alpha_o)_{\mathcal{R}}}$	Normalized fuel pressure-drop ratio, $\left(\frac{\Delta P_{If}}{P_c}\right)_{\mathcal{R}=5}$	Normalized LOX pressure-drop ratio, $\left(\frac{\Delta P_{Io}}{P_c}\right)_{\mathcal{R}=5}$
	lb_f/in^2	N/m		lb_m/sec	kg/sec											
1	295	2.03×10^6	5.03	0.488	0.221	0.770	0.678	1.44	Stable	Stable	42	103	0.997	1.00	0.677	1.4
2	303	2.09	4.90	.539	.244	.709	.832	.807			41	100	1.00	.998	.832	.805
7	300	2.07	5.12	.549	.249	.700	.450	.875			41	101	.994	1.00	.447	.875
8	300	2.07	4.95	.530	.240	.717	.450	.700			42	104	1.00	1.00	.450	.700
9	295	2.03	5.07	.542	.246	.695	.475	.678			43	105	.997	1.00	.474	.678
13	300	2.07	5.01	.536	.243	.711	.300	.850			41	102	.999	1.00	.300	.850
19	295	2.03	4.95	.555	.252	.674	.205	.881			39	99	1.00	1.00	.205	.881
20	297	2.05	5.22	.585	.265	.655	.222	.616			43	100	.998	1.01	.219	.622
30	295	2.03	5.08	.518	.235	.727	.576	.881			43	102	.996	1.00	.574	.881
34	297	2.05	4.83	.536	.243	.696	.136	.591			40	100	1.00	.998	.136	.590
36	305	2.10	4.98	.549	.249	.706	.082	.377			44	105	1.00	1.00	.820	.377
37	292	2.01	4.98	.549	.249	.676	.079	.387			42	100	1.00	1.00	.0790	.387
40	300	2.07	5.16	.506	.229	.761	.050	.315			43	100	.991	1.00	.0496	.315
45	300	2.07	5.00	.570	.258	.669	.050	.525			41	108	1.00	1.00	.0500	.525
46	298	2.05	4.86	.545	.247	.688	.047	.445			40	108	1.00	.998	.0470	.444

103	300	2.07×10^{6}	4.85	0.490	0.222	0.770	1.36	0.950	Stable	Stable	42	106	1.00	0.998	1.36	0.948
104	300	2.07	5.31	.536	.243	.726	1.36	.475	Stable	Stable	42	108	.986	1.01	1.34	.480
107	302	2.08	5.12	.522	.237	.741	1.33	.654	Stable	Stable	41	107	.994	1.00	1.32	.654
5	302	2.08	4.94	.534	.242	.715	.813	.525	Unstable	Unstable	44	106	1.00	1.00	.813	.525
6	303	2.09	5.01	.536	.243	.718	.733	.436			42	107	.999	1.00	.732	.436
11	298	2.05	4.97	.536	.243	.705	.460	.460			42	104	1.00	1.00	.460	.460
21	300	2.07	4.93	.561	.254	.676	.225	.500			45	106	1.00	1.00	.225	.500
22	295	2.03	4.94	.567	.257	.658	.246	.475			46	105	1.00	1.00	.246	.475
26	295	2.03	4.92	.561	.254	.665	.703	.170			43	107	1.00	.999	.703	.170
27	296	2.04	4.97	.552	.250	.680	.672	.252			45	108	1.00	1.00	.672	.252
29	300	2.07	4.89	.524	.238	.722	.600	.560			41	100	1.00	.998	.600	.559
14	300	2.07	5.02	.542	.246	.705	.300	.650	Stable		45	100	.998	1.00	.299	.650
15	307	2.12	5.02	.542	.246	.721	.270	.441			43	109	.998	1.00	.269	.441
16	305	2.10	4.97	.536	.243	.721	.279	.525			44	112	1.00	1.00	.279	.525
17	310	2.14	4.94	.534	.242	.734	.273	.403			44	111	1.00	1.00	.273	.403
23	295	2.03	4.88	.561	.254	.663	.220	.373			43	112	1.00	.998	.220	.372
31	295	2.03	4.95	.530	.240	.705	.155	.348			43	105	1.00	1.00	.144	.348
32	295	2.03	4.91	.545	.247	.683	.170	.388			43	105	1.00	.998	.170	.387
33	293	2.02	4.87	.540	.245	.684	.126	.526			45	101	1.00	.988	.126	.525
39	295	2.03	5.02	.583	.264	.644	.068	.170			42	110	.998	1.00	.679	.170
47	295	2.03	5.13	.585	.265	.647	.042	.271			42	107	.993	1.00	.0417	.271
48	305	2.10	4.98	.567	.257	.683	.033	.180			40	110	1.00	1.00	.033	.180
3	297	2.05	4.92	.536	.243	.700	.843	.667	Unstable	Stable	42	102	1.00	.999	.843	.666
4	300	2.07	4.96	.536	.243	.709	.825	.600			42	101	1.00	1.00	.825	.600
10	295	2.03	5.03	.539	.244	.697	.485	.551			43	100	.997	1.00	.484	.551
105	296	2.04	5.26	.542	.246	.706	1.43	.394			42	110	.987	1.01	1.41	.398
106	295	2.03	4.98	.518	.235	.723	1.40	.398			42	108	1.00	1.00	1.40	.398

TABLE IV. - ESTIMATION OF COMBUSTION DELAYS FOR ANALOG COMPUTER SIMULATION

Chamber pressure		Calculated vaporization time, msec	Calculated total delay time, msec; Hz	Required mixing time, msec	Best-fit LOX vaporization time, msec	Best-fit mixing time, msec
$lb_f/in.^2$	N/m^2					
650	4.48×10^6	4.7	6.7; 68	2.0	4.4	2.2
300	2.07	7.5	11.3; 40	3.8	8.0	4.0

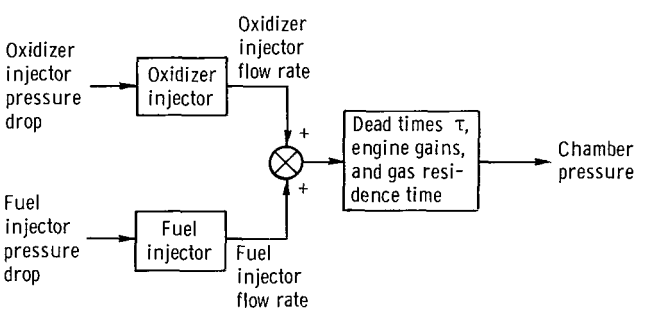

(a) Single dead-time model.

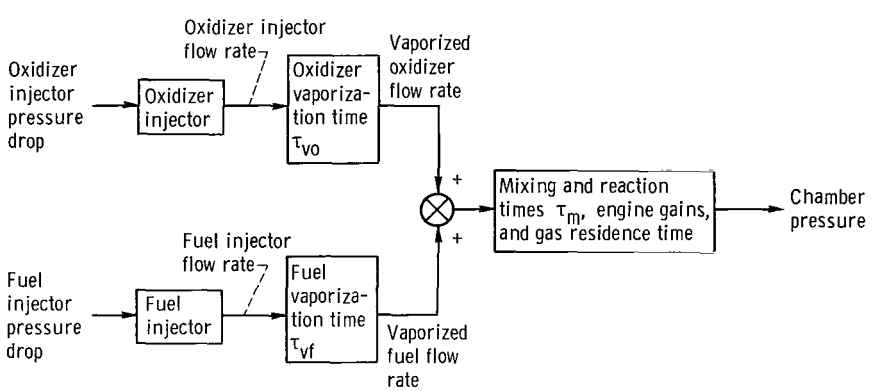

(b) Double dead-time model.

Figure 1. - Comparison of stability limit models for bipropellant rocket engines.

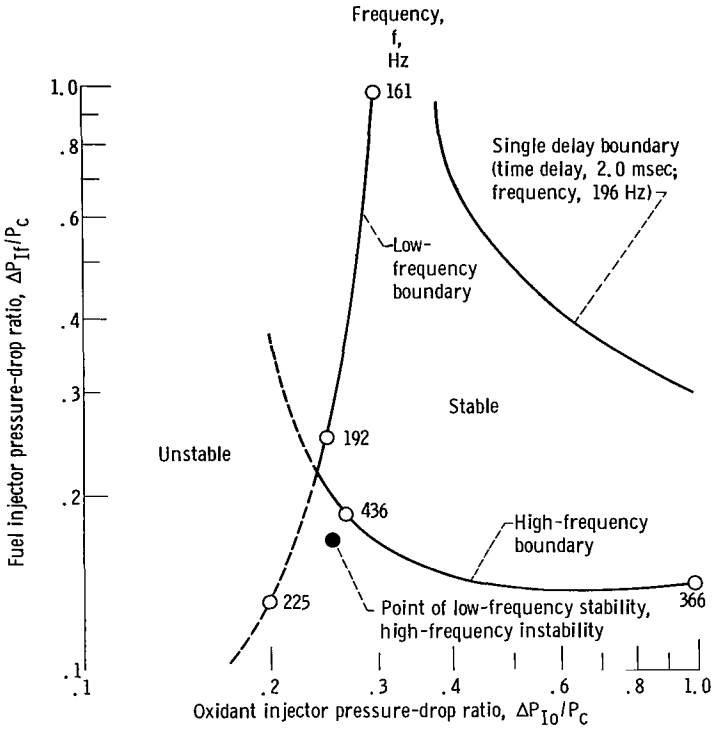

Figure 2. - Typical stability boundaries. Double dead-time model: fuel vaporization time delay, 0 millisecond; oxidizer vaporization time delay, 1.75 milliseconds; mixing time delay, 1.0 millisecond; theoretical gas residence time, 0.7 millisecond; single dead-time model: time delay, 2.0 milliseconds; theoretical gas residence time, 0.7 millisecond.

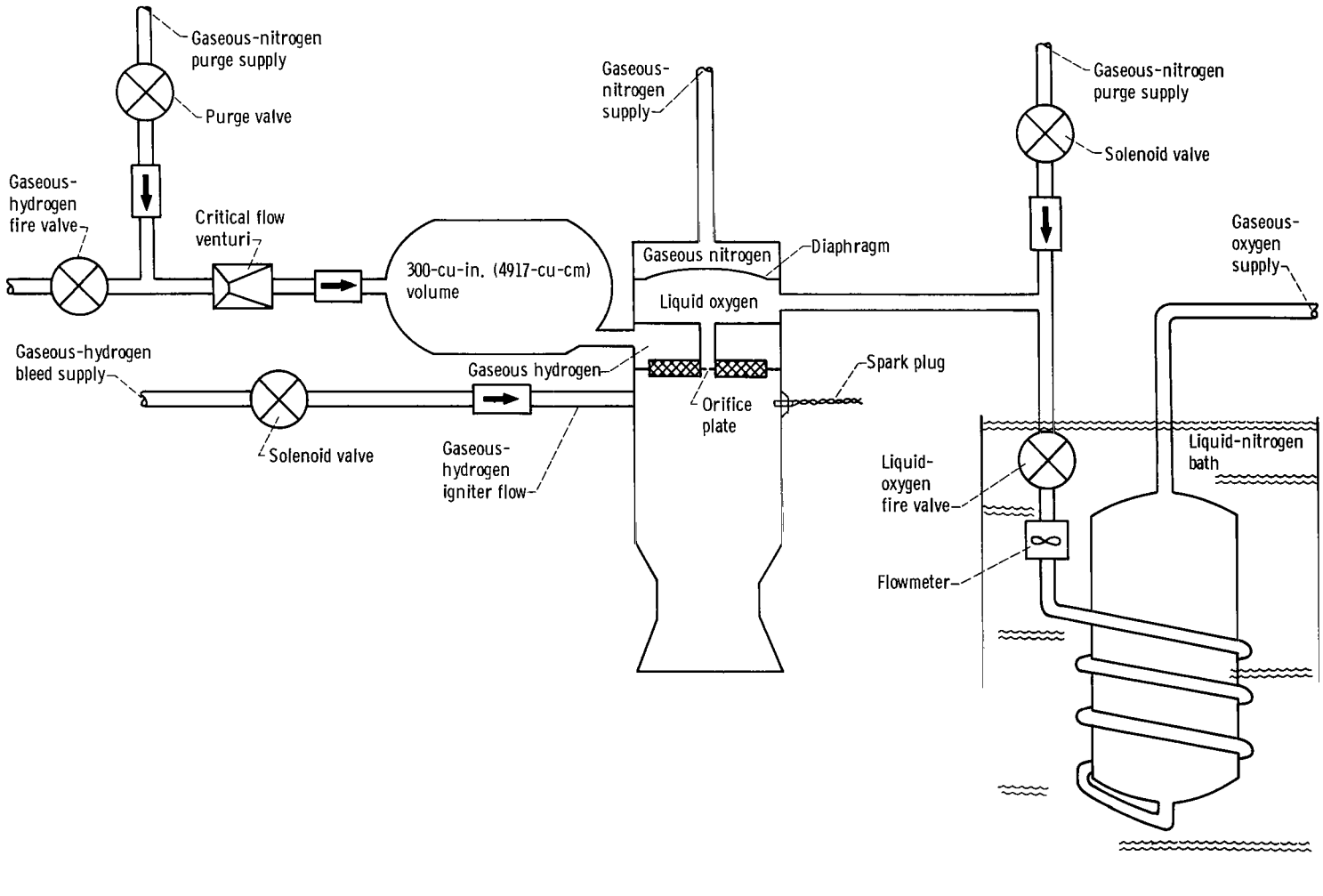

Figure 3. - Rocket combustion laboratory flow system and test engine configuration.

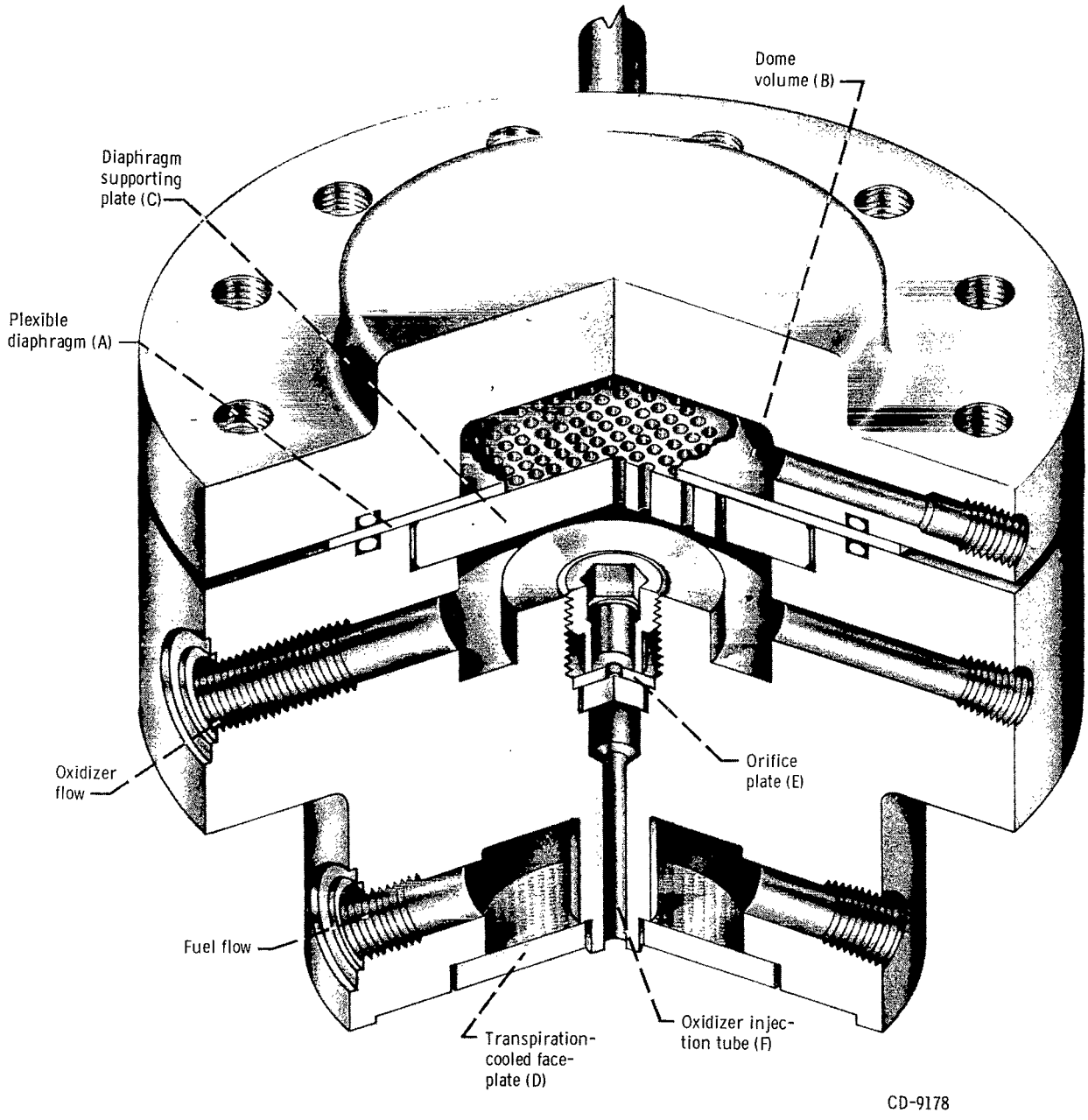

Figure 4. - Cutaway diagram of hydrogen-oxygen chugging injector.

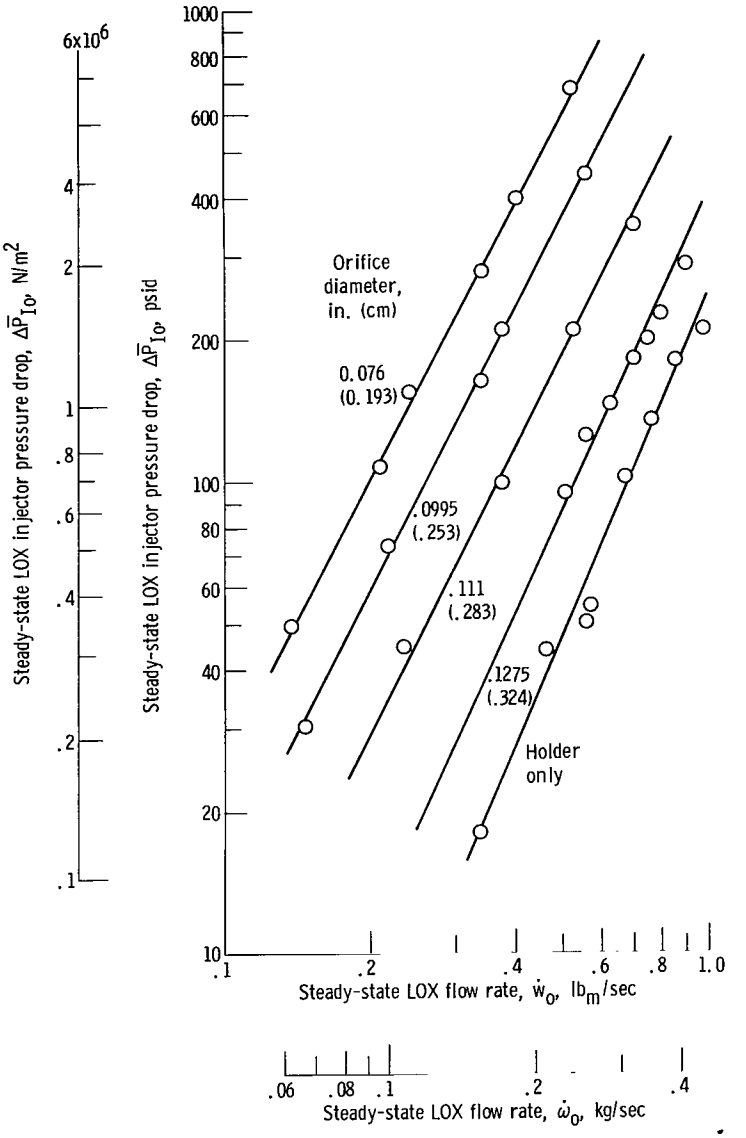

Figure 5. - Cold-flow LOX injector pressure-drop characteristics.

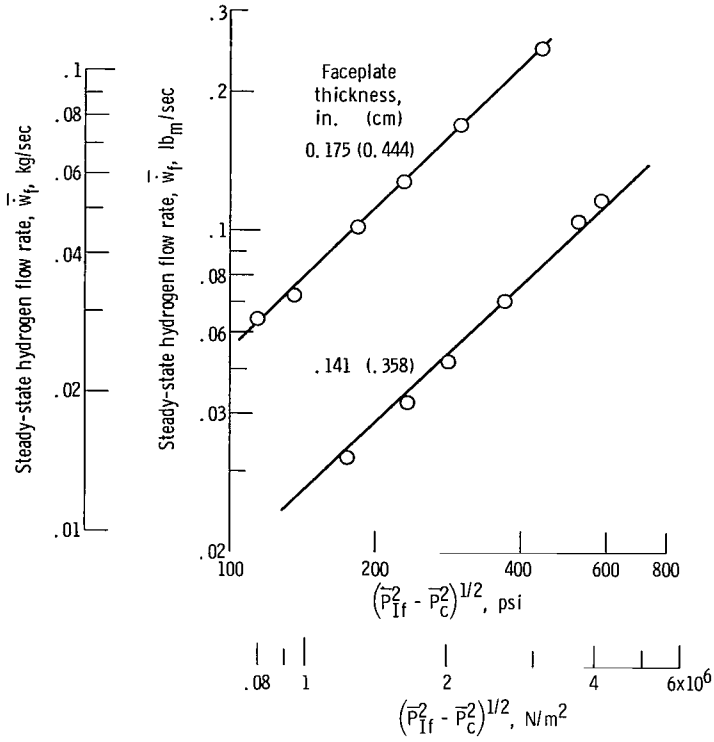

Figure 6. - Cold-flow fuel injector pressure-drop characteristics.

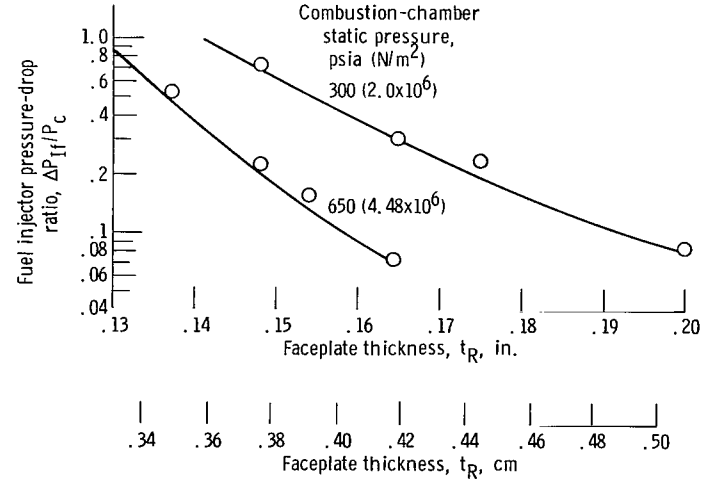

Figure 7. - Estimated fuel injector pressure-drop characteristics based on cold-flow tests. Fuel mass flow rate, 0.11 pound mass per second.

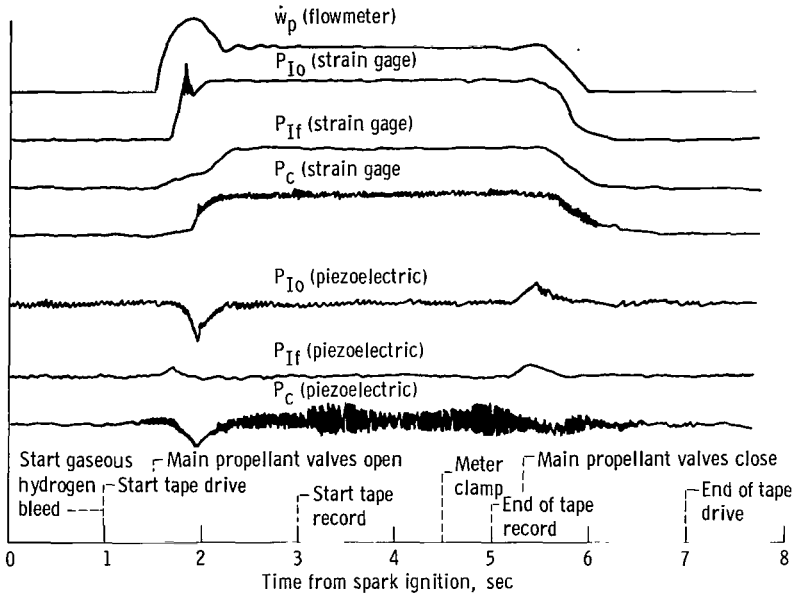

Figure 8. - Typical start transient.

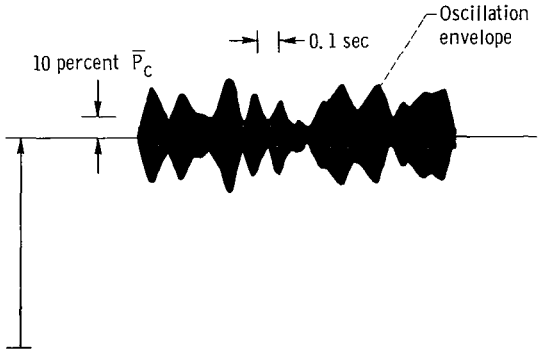

Figure 9. - Typical observed chamber-pressure oscillation during chugging. Frequency, 42 hertz.

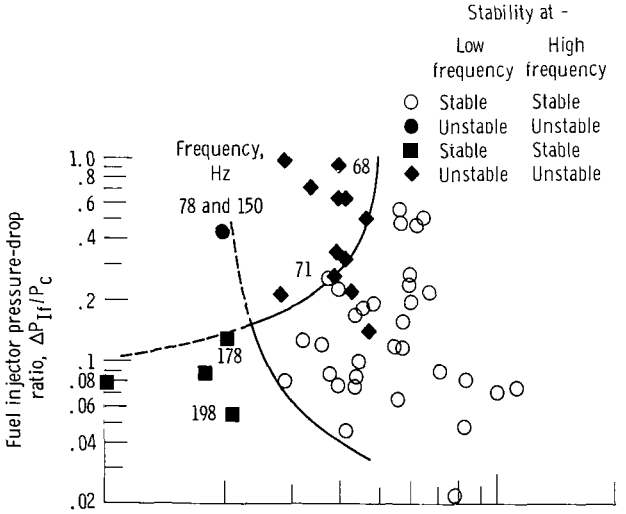

(a) Combustion-chamber static pressure, 650 psia (4.48×10^6 N/m^2); characteristic length, 91.0 inches (2.31 m); observed frequencies, 68 to 78 and 150 to 198 hertz.

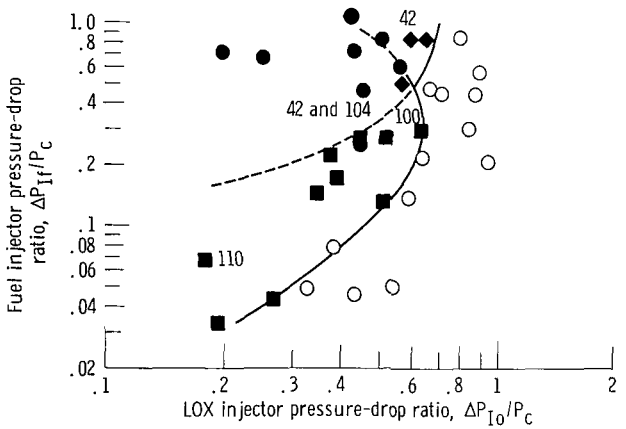

(b) Combustion-chamber static pressure, 300 psia (2.07×10^6 N/m^2); characteristic length, 95.5 inches (2.43 m); observed frequencies, 41 to 46 and 100 to 112 hertz.

Figure 10. - Experimentally determined stability boundary. Mixture ratio, 5.0; oxidizer mass flow rate, 0.55 pound mass per second (0.249 kg/sec).

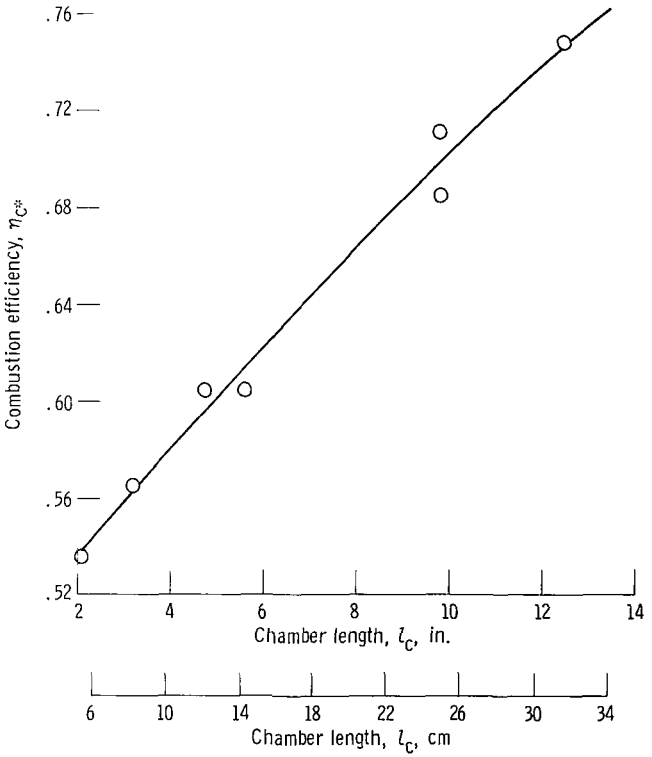

Figure 11. - Determination of length required to vaporize 50 percent of oxidizer droplet mass. Combustion-chamber static pressure, 300 psia (2.07×10^6 N/m^2); mixture ratio, 5.0; ratio of cross-sectional area of combustion chamber to that of exhaust nozzle thrust, 16.8; combustion efficiency at 50 percent, 0.616; chamber length at 50 percent, 5.5 inches (14.0 cm); oxidizer jet velocity, 735 inches per second (18.7 cm/sec); time delay at 50 percent and oxidizer vaporization time delay, 7.48 milliseconds.

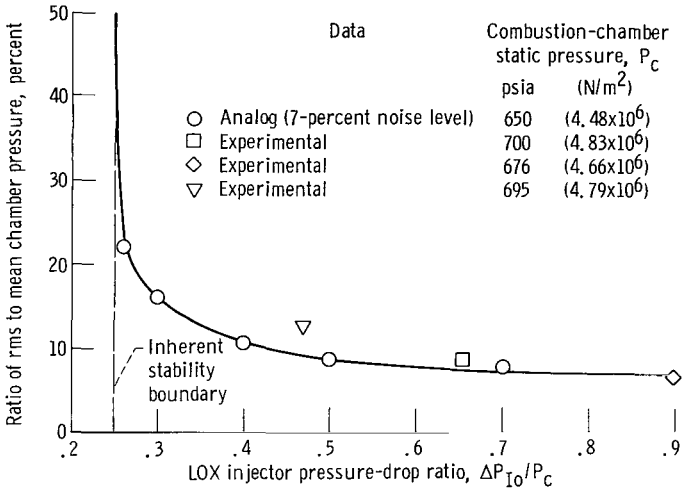

Figure 12. - Comparison of amplitudes of oscillation for experimental and simulation runs. Fuel injector pressure-drop ratio, 0.500; selected noise level.

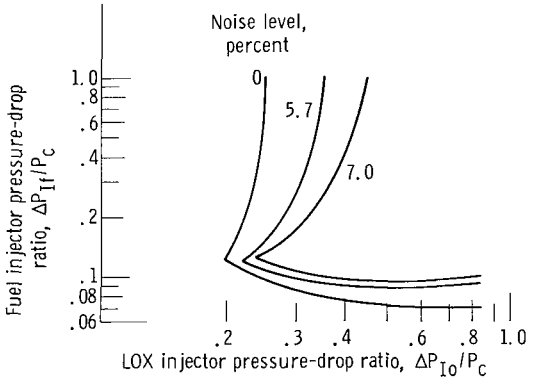

Figure 13. - Effect of noise level on simulation stability boundary. Combustion-chamber static pressure, 650 psia $(4.48x10^6\ N/m^2)$; fuel vaporization time delay, 0; oxidizer vaporization time delay, 4.4 milliseconds; mixing time delay, 2.2 milliseconds; theoretical gas residence time, 2.0 milliseconds.

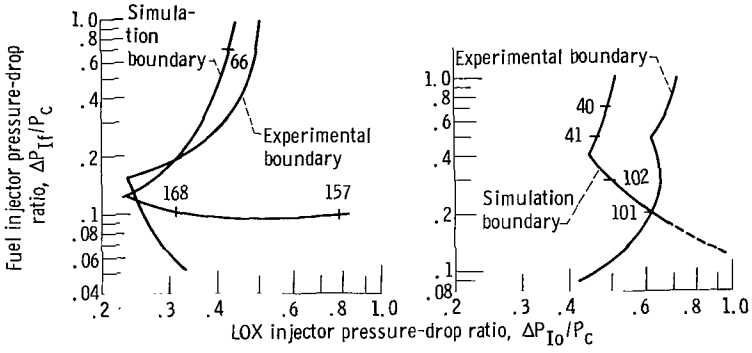

(a) Combustion-chamber static pressure, 650 psia (4.48x10^6 N/m^2); oxidizer vaporization time delay, 4.4 milliseconds; mixing time delay, 2.2 milliseconds; theoretical gas residence time, 2.0 milliseconds.

(b) Combustion-chamber static pressure, 300 psia (2.07x10^6 N/m^2); oxidizer vaporization time delay, 8.0 milliseconds; mixing time delay, 4.0 milliseconds; theoretical gas residence time, 2.1 milliseconds.

Figure 14. - Comparison of experimental and simulation stability boundaries. Fuel vaporization time delay, 0; noise level, 7 percent.

NATIONAL AERONAUTICS AND SPACE ADMINISTRATION
WASHINGTON, D.C. 20546
OFFICIAL BUSINESS

FIRST CLASS MAIL

POSTAGE AND FEES PAID
NATIONAL AERONAUTICS AND
SPACE ADMINISTRATION

"The aeronautical and space activities of the United States shall be conducted so as to contribute . . . to the expansion of human knowledge of phenomena in the atmosphere and space. The Administration shall provide for the widest practicable and appropriate dissemination of information concerning its activities and the results thereof."

—NATIONAL AERONAUTICS AND SPACE ACT OF 1958

NASA SCIENTIFIC AND TECHNICAL PUBLICATIONS

TECHNICAL REPORTS: Scientific and technical information considered important, complete, and a lasting contribution to existing knowledge.

TECHNICAL NOTES: Information less broad in scope but nevertheless of importance as a contribution to existing knowledge.

TECHNICAL MEMORANDUMS: Information receiving limited distribution because of preliminary data, security classification, or other reasons.

CONTRACTOR REPORTS: Scientific and technical information generated under a NASA contract or grant and considered an important contribution to existing knowledge.

TECHNICAL TRANSLATIONS: Information published in a foreign language considered to merit NASA distribution in English.

SPECIAL PUBLICATIONS: Information derived from or of value to NASA activities. Publications include conference proceedings, monographs, data compilations, handbooks, sourcebooks, and special bibliographies.

TECHNOLOGY UTILIZATION PUBLICATIONS: Information on technology used by NASA that may be of particular interest in commercial and other non-aerospace applications. Publications include Tech Briefs, Technology Utilization Reports and Notes, and Technology Surveys.

Details on the availability of these publications may be obtained from:

SCIENTIFIC AND TECHNICAL INFORMATION DIVISION

NATIONAL AERONAUTICS AND SPACE ADMINISTRATION

Washington, D.C. 20546